Experimental Analysis of Tip Vibrations at Higher Eigenmodes of QPlus Sensors for Atomic Force Microscopy

Michael G. Ruppert[1], Daniel Martin-Jimenez[2,3], Yuen K. Yong[1], Alexander Ihle[2,3], André Schirmeisen[2,3], Andrew J. Fleming[1], and Daniel Ebeling[2,3]

[1]School of Engineering, University of Newcastle, Callaghan, NSW, 2308, Australia
[2]Institute of Applied Physics, Justus Liebig University Giessen, Giessen, Germany
[3]Center for Materials Research, Justus Liebig University Giessen, Giessen, Germany

E-mail:
michael.ruppert@newcastle.edu.au,Daniel.Ebeling@ap.physik.uni-giessen.de

October 2021

Abstract. QPlus sensors are non-contact atomic force microscope probes constructed from a quartz tuning fork and a tungsten wire with an electrochemically etched tip. These probes are self-sensing and offer an atomic-scale spatial resolution. Therefore, qPlus sensors are routinely used to visualize the chemical structure of adsorbed organic molecules via the so-called bond imaging technique. This is achieved by functionalizing the AFM tip with a single CO molecule and exciting the sensor at the first vertical cantilever resonance mode. Recent work using higher-order resonance modes has also resolved the chemical structure of single organic molecules. However, in these experiments, the image contrast can differ significantly from the conventional bond imaging contrast, which was suspected to be caused by unknown vibrations of the tip. This work investigates the source of these artefacts by using a combination of mechanical simulation and laser vibrometry to characterize a range of sensors with different tip wire geometries. The results show that increased tip mass and length cause increased torsional rotation of the tuning fork beam due to the off-center mounting of the tip wire, and increased flexural vibration of the tip. These undesirable motions cause lateral deflection of the probe tip as it approaches the sample, which is rationalized to be the cause of the different image contrast. The results also provide a guide for future probe development to reduce these issues.

Keywords: Atomic force microscopy, qPlus sensor, tuning fork sensor, bond imaging technique, higher eigenmodes, modal analysis. Submitted to: *Nanotechnology*

1. Introduction

The atomic force microscope (AFM) [1] has become a key enabling technology for advances in chemistry [2], surface physics [3] and bio-nanotechnology [4]. With the capture of the image of the chemical structure of an organic molecule for the first time in 2009 [2], it became possible to visualize the molecular wire frame model with distinct contrast of the chemical bonds between bonded atoms. In order to achieve these extreme resolutions, the 'bond imaging' technique is often used to resolve the chemical structure of single adsorbed molecules [2]. In this method, the AFM tip is functionalized with a single CO molecule at the tip apex which significantly increases the lateral resolution. Successful applications of this method include the identification of intermolecular bonding configurations [5], direct imaging of the molecular bond structure [6], measuring the length of molecular bonds [7–9], and investigating single-molecule reaction chains [6, 10–13]. Furthermore, the AFM tip can serve as a tool to build bespoke organic nano-architectures in a molecule by molecule fashion [14].

In order to resolve the chemical structure of single molecules using the bond imaging technique, the atomic force microscope is mainly operated in non-contact frequency modulation mode in ultra-high vacuum and at low temperatures [15]. In this mode, the frequency of the oscillating sensor is altered by the gradient of the tip sample force and provides the imaging channel for topographic information. Due to the excellent frequency stability and high stiffness required to achieve small oscillation amplitudes, the qPlus sensor has become the leading instrument to image with atomic and sub-atomic spatial resolution [16–18]. Originally based on a tuning fork from wrist watches used for time keeping, the qPlus sensor also provides an integrated displacement signal due to the piezoelectric effect of the quartz material. The ability to establish a tunnelling current between the qPlus sensor tip and sample also enables combined atomic force and scanning tunnelling microscopy [19].

Conventionally, the qPlus sensor is operated at the first vertical mode (in the direction of the tip) but recently higher eigenmodes of the qPlus sensor are being investigated for high resolution imaging. Driving silicon cantilevers at the second eigenmode has been demonstrated to yield atomic resolution in ultra-high vacuum [20] and liquids [21]. A similar trend is exhibited by the higher eigenmodes of qPlus sensors, which were shown to resolve the lattice structure of ionic crystal surfaces in vacuum [22], ambient conditions [23], and liquids [24]. However, recent studies also revealed that the tip geometry of the qPlus sensor can have a crucial impact on the imaging contrast, particularly when using higher eigenmodes for imaging [25]. Longer tip shapes have the potential to significantly increase the imaging contrast; however, phenomena such as contrast reversal remain unexplained [26]. Single chemical bonds have recently been imaged with unprecedented resolution using the lateral oscillations of the CO-terminated tip [27]. Another variation includes the combination of vertical and axial oscillation, which requires an alternative electrode configuration [28].

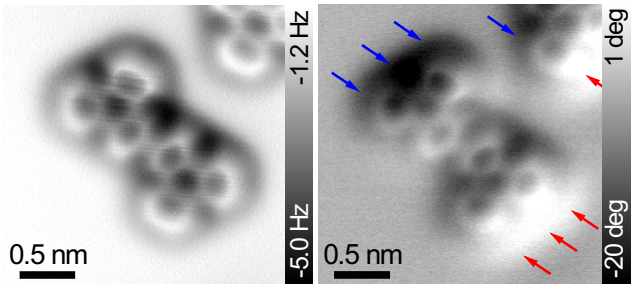

(a) Vertical Mode 1 (b) Vertical Mode 2

Figure 1. Constant-height AFM images of a bitriphenylene molecule on Ag(111). (a) Frequency shift image obtained by exciting the qPlus sensor at the first vertical eigenmode (f_1 = 26.96 kHz). (b) Phase shift image obtained by exciting the second vertical eigenmode (f_2 = 163.96 kHz). The blue and red arrows indicate dark and bright features, which are only observed when operating the sensor at the second vertical eigenmode.

Recently it was observed that the higher eigenmodes of qPlus sensors are capable of resolving the internal bonding structure of adsorbed organic compounds [26]. The contrast of the higher eigenmode images is, however, somewhat different from the conventional image contrast. Figure 1 depicts two exemplary AFM images of a bitriphenylene molecule on a Ag(111) surface, which were taken by exciting either the first or the second vertical eigenmode of the qPlus sensor. The conventional bond image shown in Figure 1(a) reveals a rather similar level of brightness for all C-C bonds (in other words, the molecule looks planar). The second eigenmode image in Figure 1(b), on the contrary, shows some dark and bright regions at the upper left and lower right of the scanned molecule,

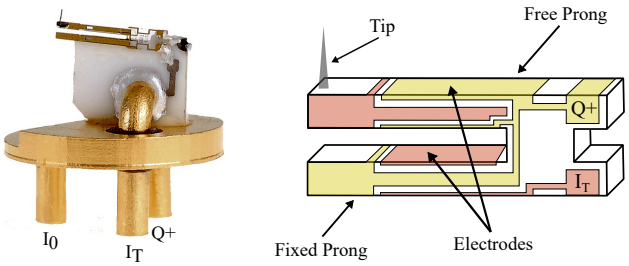

Figure 2. Photo (source: Scienta Omicron) and schematic electrode layout of a second generation qPlus sensor.

as indicated by the blue and red arrows. Therefore, it appears the molecule is bent downward towards the surface at the dark region (blue arrows) and bent upwards at the bright region (red arrows). Presumably, these image features are caused by an additional lateral tip oscillation (in the direction of the red and blue arrows) that is overlayed with its vertical oscillation.

The aforementioned discussion highlights the importance of understanding precisely the vibrational mode shapes of the qPlus sensor. Particularly, when higher eigenmodes and lateral vibrational modes are used to obtain high resolution images, the origin of imaging contrast has not been fully examined. In most conventional high-resolution AFM setups, the qPlus sensor is actuated acoustically and the tip displacement is measured using the piezoelectric effect of the quartz material. However, this approach introduces a multitude of additional dynamics which make the identification of sensor modes exceedingly difficult. In this work, the vibrational mode shapes of a second generation qPlus sensor are experimentally measured using laser Doppler vibrometry. The measurement methods are similar to that used for the characterization of microelectromechanical systems [29, 30]. Four different qPlus sensors (tip-less, glue-only, short tip, and long tip, see Figure 4) are measured to compare their frequency responses, quality factors, and deflection mode shapes. The results match finite element simulations and demonstrate significant lateral deflections of the tip.

2. The qPlus Tuning Fork Sensor

A photo of a second generation qPlus sensor [31] and schematic drawing of the electrode layout is shown in Figure 2. One prong of the tuning fork is glued (EPO-TEK H70E-2) to a macor substrate and the other prong is used as the tip carrier and is free to move. Two electrodes are arranged around the prong such that the electric field vectors are pointing to opposite directions in the upper and lower halves of the cross section [31]. As a result, the vertical

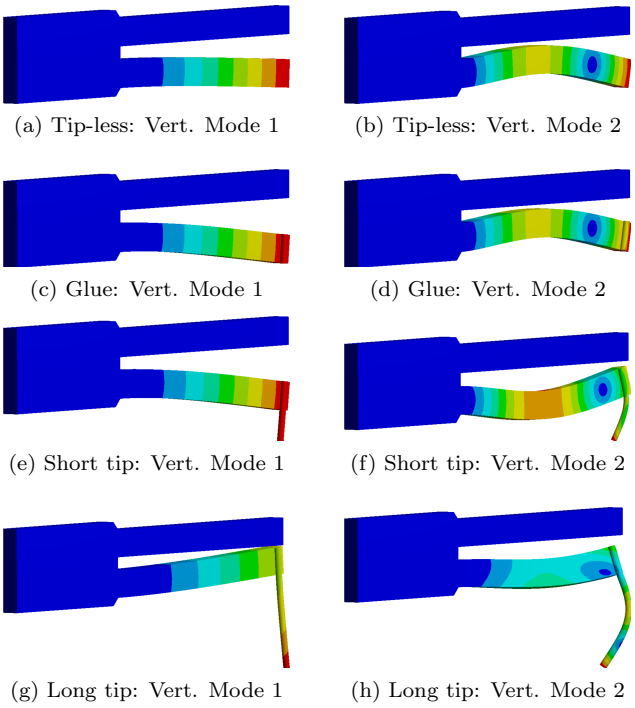

Figure 3. Finite element simulation of the qPlus sensors. First and second vertical mode shape of the (a)-(b) tip-less, (c)-(d) glue-only, (e)-(f) short-tip, and (g)-(h) long-tip qPlus sensor.

electrodes and the lateral electrodes develop surface charges of opposite polarity. Since one prong of the tuning fork is fixed to the substrate, the other prong effectively behaves like a cantilever and shows eigenmodes predicted by Euler-Bernoulli beam theory [25]. Needles made of electrochemically sharpened tungsten wires are attached to the free end of the prong using conductive glue (EPO-TEK E2101). Since the quartz qPlus sensor material is piezoelectric, a surface charge on the electrodes is generated if the prong is deflected. This surface charge can be measured by using a low-noise current amplifier connected to the $Q+$ terminal [32] while grounding the shield electrode I_0. The qPlus sensor tip is electrically connected to the electrode I_T which allows the additional measurement of the tunnelling current [19].

3. Finite Element Analysis

Numerical finite element simulations of the four types of qPlus sensors were performed using the modal analysis module of Ansys Workbench. The dimensions of the qPlus sensor and material properties were taken from [25]. In the simulations, the peak deflection of each eigenmode representing the deflection of the i^{th} resonance frequency is normalized to 1. The simulated resonance frequencies are stated in Table 1. The first and second vertical resonance modes are observed

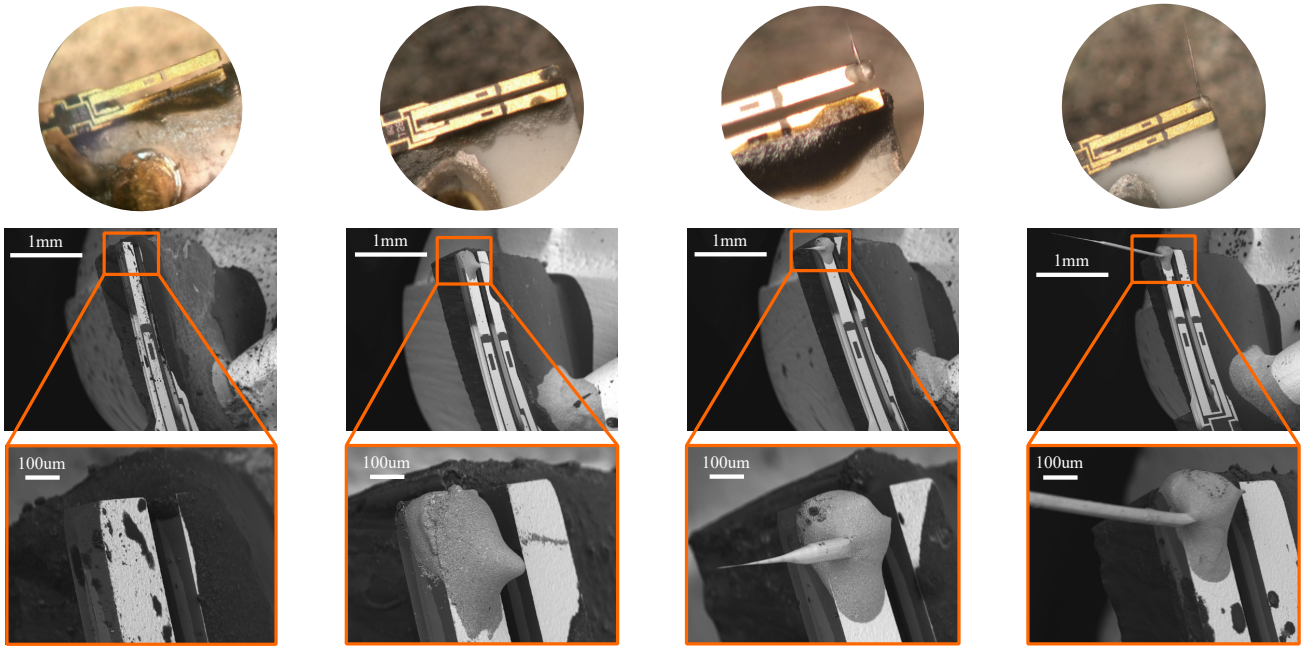

(a) Tipless qPlus Sensor (b) Glue Only qPlus Sensor (c) Short Tip qPlus Sensor (d) Long Tip qPlus Sensor

Figure 4. Optical and SEM images of the experimentally investigated qPlus sensors. (a) A tip-less qPlus sensor, (b) a qPlus sensor with glue-only (EPO-TEK E2101), (c) a qPlus sensor with a short tip (tungsten wire) and (d) a qPlus sensor with a long tip (tungsten wire).

to reduce in frequency as the attached tip mass is increased.

The resonance mode shapes are shown in Figure 3. The first vertical mode of the tip-less, glue-only and short-tip qPlus sensor do not show significant lateral deflection of the prong or the tip. However, the long-tip qPlus sensor exhibits lateral tip deflection and torsional rotation of the prong at the first vertical mode. The second vertical mode of the tip-less and glue-only qPlus sensors do not show any torsional rotation of the prong, but the short-tip and long-tip qPlus sensor show significant lateral tip deflection. This will be analysed in more detail in Section 4.6.

4. Experimental Analysis

In this section, four different qPlus sensors are analysed experimentally. All sensors are second generation qPlus sensors [31] with one prong glued to a macor substrate with electrodes for electrical connections. The sensors vary in their tip condition as shown in Figure 4. In the following, the effect of the tip conditions on the eigenmodes is investigated by recording the frequency response function, the thermal noise response and the deflection mode-shapes. These recordings are used to identify the actuator and sensor sensitivities and dynamic parameters of the qPlus sensor eigenmodes. Additionally, the lateral tip deflections are measured at the first and second vertical mode as well as at the second lateral mode.

4.1. Experimental Setup

The three experimental setups required to measure the electrical and mechanical responses are illustrated in Figure 5. The setups contain a custom-built probe station with a piezoelectric stack actuator and a current pre-amplifier to measure the sensor signal. This setup is similar to that used in a commercial AFM. In the following, the qPlus sensors are either actuated acoustically using the piezoelectric stack actuator or electrically via direct piezoelectric excitation of the quartz tuning fork. The responses are either measured electrically using the current pre-amplifier or optically using a laser Doppler vibrometer (Polytec, MSA-100-3D).

In the measurement setup in Figure 5(a), the qPlus sensor response is obtained by exciting the piezoelectric stack actuator with a sine sweep and measuring the response using a lock-in amplifier (Zurich Instruments, HF2LI). In this scheme, the qPlus sensor is excited acoustically. This measurement reveals the location of the first vertical resonance frequency; however, the second resonance frequency is difficult to identify due to the numerous additional structural modes.

In the measurement setup shown in Figure 5(b), the tuning fork is excited acoustically as in Figure 5(a)

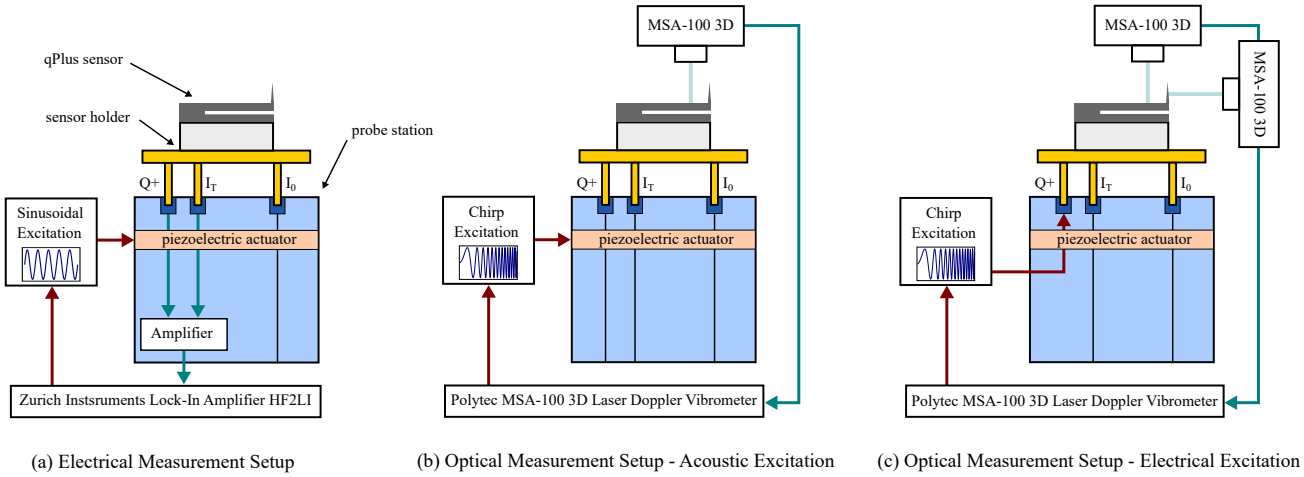

(a) Electrical Measurement Setup (b) Optical Measurement Setup - Acoustic Excitation (c) Optical Measurement Setup - Electrical Excitation

Figure 5. Experimental setups. The electrical measurement setup (a) is used for measuring the frequency response using the integrated current pre-amplifier. The optical measurement setups (b) and (c) are used to measure the frequency responses using a laser Doppler vibrometer and to measure the beam and tip mode shapes. In (c), the rotated MSA-100 scan head indicates lateral measurements of the qPlus sensors. Actuation signal chains are highlighted red and sensor signal chains are highlighted green.

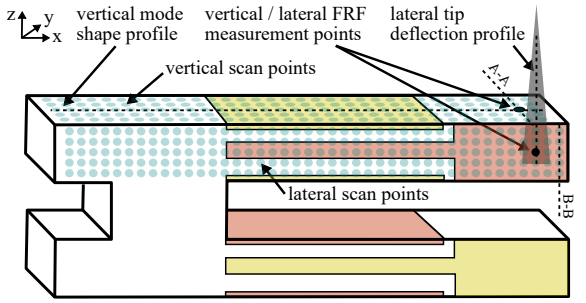

Figure 6. Scan point layout. Schematic of the measurement points for the lateral (y-direction) and vertical (z-direction) bending mode measurements.

but with a periodic chirp signal. In contrast, the measurement setup shown in Figure 5(c) employs direct piezoelectric excitation of the sensor via the $Q+$ electrode. In this scheme, the qPlus sensor is excited electrically. The resulting mechanical response of the sensor is measured with a laser Doppler vibrometer (Polytec, MSA-100-3D) from the top of the tuning fork (vertical measurements) and from the side of the tuning fork (lateral measurements). The location and layout of the scan points are shown in Figure 6. By comparing the electrical and optical measurement with piezoelectric stack actuation, the sensor sensitivities and exact location of the second eigenmode can be obtained. To measure the dynamic stiffness of the qPlus sensors at the first and second vertical mode, a thermal noise response is also captured with the piezoelectric stack actuator grounded. Thermal noise responses are shown and analyzed in Section Appendix B. Lastly, the lateral tip vibrations of the qPlus sensors at the first and second vertical mode are measured by rotating the probe station by 90 degrees with respect to the laser Doppler vibrometer.

Table 1. Simulated and experimentally determined first and second vertical mode resonance frequencies of the qPlus sensors.

Sensor	Simulation		Experiment	
	$f_{1,v}$ [kHz]	$f_{2,v}$ [kHz]	$f_{1,v}$ [kHz]	$f_{2,v}$ [kHz]
Tip-less	32.3	195.1	32.69	197.0
Glue	32.0	193.9	29.04	182.7
Short Tip	23.2	169.5	23.50	179.3
Long Tip	16.5	173.3	21.37	156.4

4.2. Frequency Response Analysis

The frequency responses of the four qPlus sensors are shown in Figure 7. The responses were measured by exciting the piezoelectric stack actuator (acoustic actuation) and measuring the response from the integrated current pre-amplifier (yellow curve) and using the laser Doppler vibrometer (blue curve). Additionally, the qPlus sensors were excited directly from the $Q+$ electrode (electrical actuation) and the response was measured with the laser Doppler vibrometer (red and purple curves for vertical and lateral measurements, respectively). It can be seen that the acoustic actuation yields numerous additional dynamics in the frequency response due to the excitation of structural modes associated with the mounting structure. These modes are not related to the qPlus sensor bending modes and complicate the identification of the second eigenmode. When directly exciting the quartz tuning fork, only the bending modes of the sensor are excited as highlighted in Figure 7. As expected, the addition of an increasing

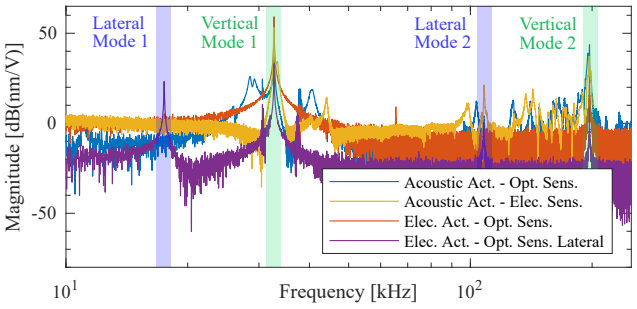

(a) Tip-less

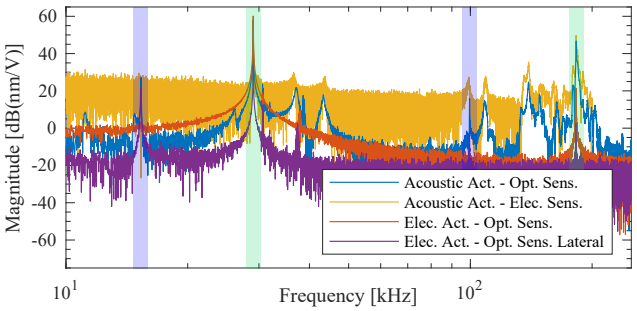

(b) Glue

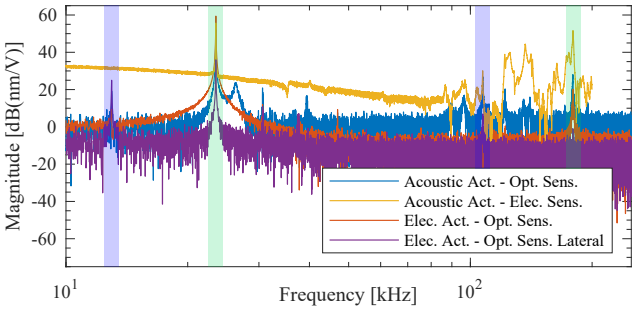

(c) Short Tip

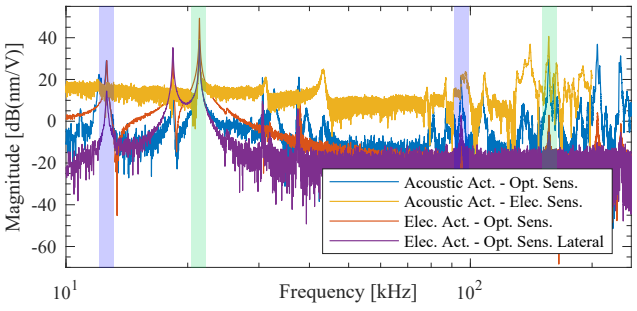

(d) Long Tip

Figure 7. Frequency responses of the qPlus sensors. Lateral resonance frequencies are highlighted in blue and vertical resonance frequencies are highlighted in green. The optical measurements are taken at the FRF measurement points as highlighted in Figure 6.

mass due to glue in (b), short tip (c) and long tip (d) leads to a reduction in the resonance frequencies, which are summarized in Table 1. Note that the long-tip qPlus sensor exhibits a split first vertical mode,

Table 2. Q factor and sensitivity of the first and second vertical mode.

Vertical Mode 1			
Sensor	Q (mech.)	Sens. (mech.) [nm/V]	Sens. (elec.) [nm/V]
Tip-less	1867	460.3	1018
Glue	2097	788.8	1013
Short Tip	1646	608.2	1006
Long Tip	512.7	91.25	304.3
Vertical Mode 2			
Sensor	Q (mech.)	Sens. (mech.) [nm/V]	Sens. (elec.) [nm/V]
Tip-less	821.5	152.2	31.18
Glue	615.0	218.0	11.81
Short Tip	585.0	24.90	10.19
Long Tip	298.3	31.04	1.397

which is due to the interaction between the prong and tip. In this case, the tip is acting like a lightly damped tuned-mass damper [33].

The acoustic and electric sensitivities at the first and second vertical modes are stated in Table 2. The Q factors are identified by fitting the magnitude response of a harmonic oscillator in a narrow bandwidth around the resonance and are also stated in Table 2. The details of this approach are described in Section Appendix A.

At the first vertical mode, the electrical excitation is more effective than the acoustic excitation and hence yields a higher sensitivity. However, at the second vertical mode the electrical excitation is less effective than the acoustic excitation. This is believed to be due to the nodal location of the second bending mode which leads to sub-optimal piezoelectric actuation [34, 35].

4.3. First and Second Lateral Bending Modes

The first eigenmode of the qPlus sensor is a lateral bending mode, also referred to as an out-of-plane bending (OPB) mode in related literature [36]. This mode is usually not observed with the integrated current amplifier nor an optical measurement from the qPlus sensor tip side. The mode is measured by rotating the qPlus sensor by 90 degrees with respect to the laser Doppler vibrometer, which results in the lateral scan point layout shown in Figure 6. The mode shapes of the tip-less and short-tip qPlus sensors are shown in Figure 8(a) and (b). The frequency response taken at the measurement point shown in Figure 6 is plotted in Figure 8(e). Here, the peaks corresponding to the first lateral eigenmode can be easily identified. Note that the first vertical bending mode is also clearly visible in the frequency response and the spurious peaks at approximately 31 kHz and 37.5 kHz are laser noise of the vibrometer. The identified resonance

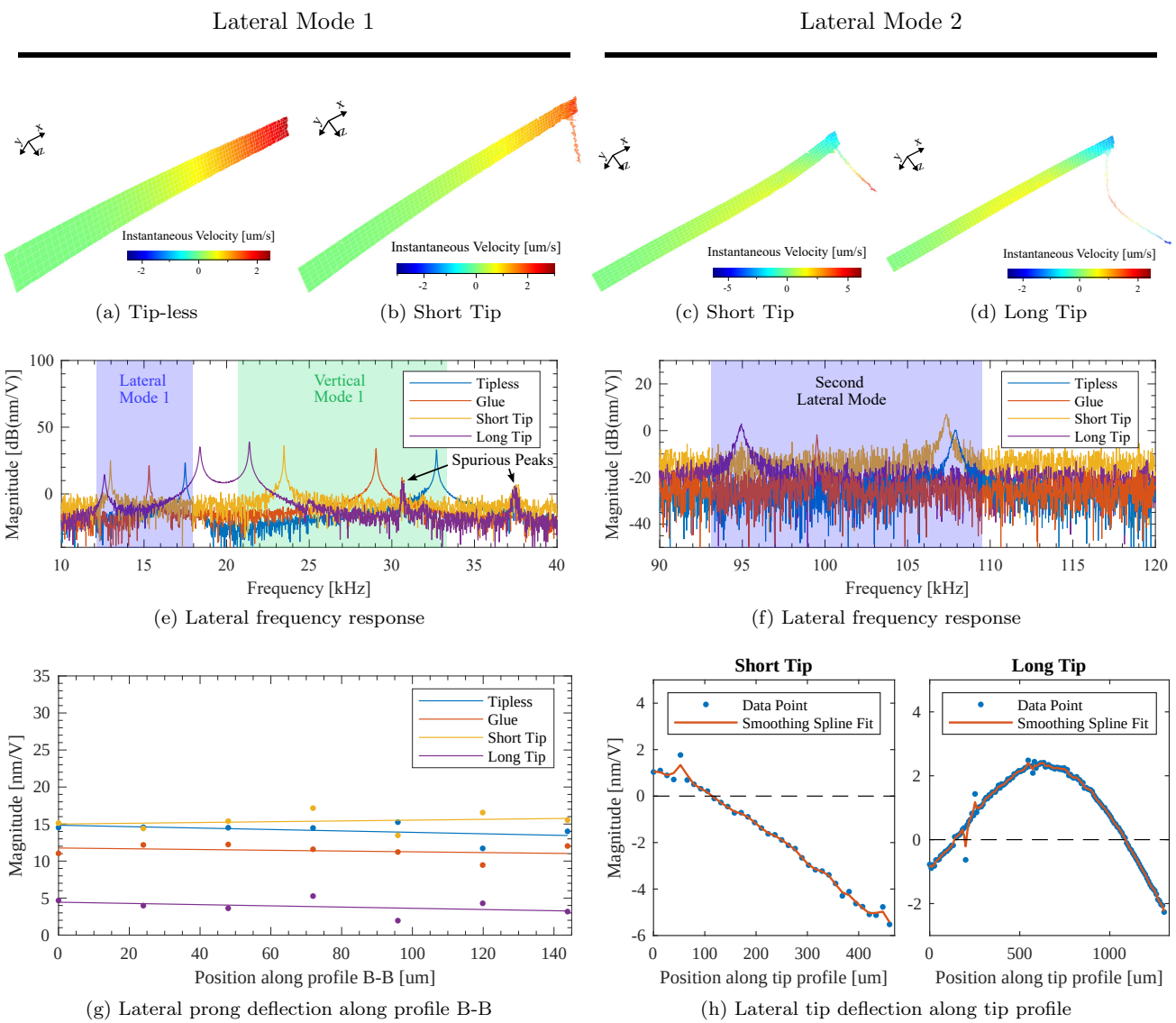

Figure 8. Experimental first and second lateral bending mode of the qPlus sensors under electrical excitation. 3D mode shapes of the first lateral bending mode of the (a) tip-less and (b) short-tip qPlus sensors. 3D mode shapes of the second lateral bending mode of the (c) short-tip and (d) long-tip qPlus sensors. Lateral frequency responses around the (e) first and (f) second lateral bending mode measured at the lateral FRF measurement point indicated in Figure 6. (g) Magnitude at the first lateral resonance frequency along the line B-B indicated in Figure 6, dots are data points and solid lines indicate linear fits to the data. (h) Lateral tip deflection profile at the second lateral bending mode of the short-tip and long-tip qPlus sensor.

frequencies, Q factors and actuation sensitivities are stated in Table 3.

By evaluating the frequency responses along the line B-B indicated in Figure 6, any torsional rotation of the prong at the lateral bending mode can be observed. This is shown in Figure 8(g) where the magnitude of the frequency response evaluated at the resonance frequency of the lateral mode is plotted against the scan point along the line B-B. It can be seen that the sensitivity is constant along the scan points which indicates the absence of torsional rotation of the prong, even for larger tip masses.

The second lateral bending mode is situated between the first and second vertical resonance frequencies and is sometimes unobservable with the current amplifier or an optical measurement from the tip side. The mode shapes for the short-tip and long-tip qPlus sensors are shown in Figure 8(c) and (d). The frequency response taken at the lateral measurement point shown in Figure 6 is shown in Figure 8(f). It reveals the peaks of the second lateral eigenmode of the four different qPlus sensors. The identified resonance frequencies, Q factors and actuation sensitivities are stated in Table 3.

By evaluating the frequency responses along the tip profile line indicated in Figure 6, the mode shape of

Table 3. Resonance frequencies, Q factors and actuation sensitivities of the first and second lateral bending mode.

Lateral Mode 1			
Sensor	$f_{1,l}$ [kHz]	$Q_{1,l}$	Sens. (elec.) [nm/V]
Tip-less	17.48	747	18.75
Glue	15.30	972	17.79
Short Tip	12.97	611	17.82
Long Tip	12.61	189	5.41
Lateral Mode 2			
Sensor	$f_{2,l}$ [kHz]	$Q_{2,l}$	Sens. (elec.) [nm/V]
Tip-less	107.9	404	1.023
Glue	99.52	1113	0.747
Short Tip	107.3	434	2.141
Long Tip	94.92	288	1.251

the tip is observed. This is shown in Figure 8(h) where the magnitude of the frequency responses evaluated at the second lateral resonance frequency is plotted against the scan points along the tip length. Both sensors show significant lateral tip deflections.

4.4. First and Second Vertical Bending Modes

The vertical bending mode shapes at the first and second vertical resonance frequency of the qPlus sensors have been measured by scanning the laser Doppler vibrometer over the top surface of the free prong using the vertical scan point layout shown in Figure 6. The resulting 3D mode shapes of the first and second vertical mode for the tip-less qPlus sensor are shown in Figure 9(a) and (b). The 2D mode shape profiles are extracted along the line indicated in Figure 6 and plotted in Figure 9(c).

It can be noticed that the mode shape of the first vertical mode is not significantly affected by the increase in tip mass. This result is in agreement with previous findings [25]. However, the node of the second mode shape moves towards the free-end as the tip mass increases. This result is also in agreement with previous findings [25]. The change in the position of the node has an effect on the piezoelectric actuation gain and sensor sensitivity. As the node moves further toward the tip, the displacement mode shape minima also moves closer to the tip. From a charge perspective, the integral over the strain mode shape is zero at this minima. As a result, the sensor sensitivity can go up or down depending on how far the electrodes extend to the end of the prong.

By evaluating the frequency responses along the line A-A indicated in Figure 6, any torsional rotation of the prong at the resonance frequencies can be observed. This is shown in Figure 9(d) for the first and second

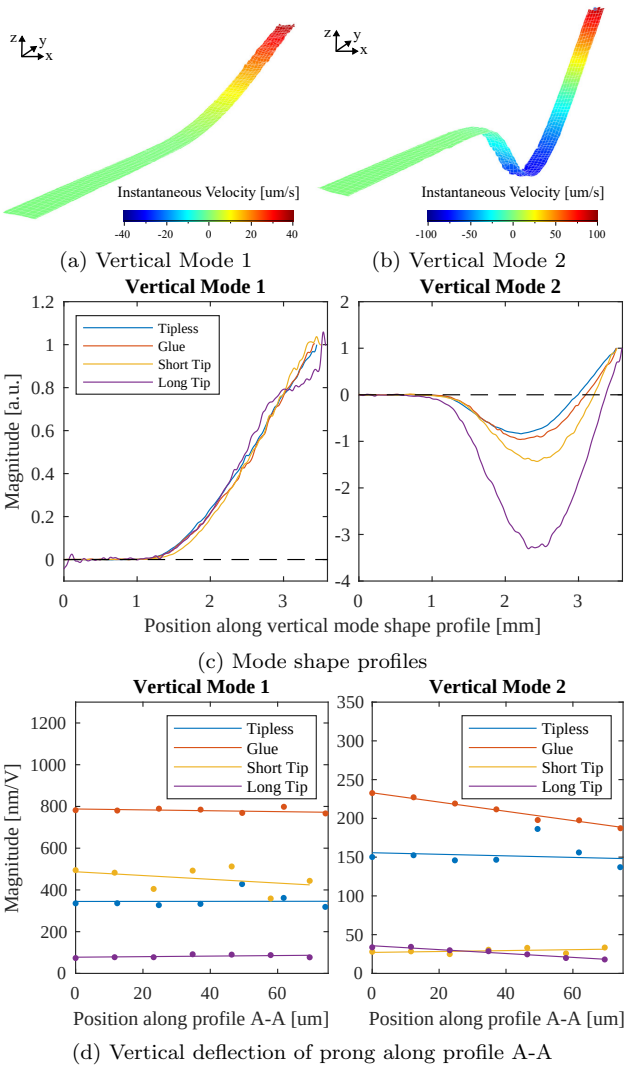

(a) Vertical Mode 1 (b) Vertical Mode 2

(c) Mode shape profiles

(d) Vertical deflection of prong along profile A-A

Figure 9. Experimental vertical mode shapes of the qPlus sensors under acoustic excitation. 3D modeshapes of the (a) first and (b) second vertical mode of the tip-less qPlus sensor. (c) Line profiles of the first and second vertical mode extracted axially along the top side of the Q-Plus sensors, tip deflection is scaled to unity. (d) Magnitude at the vertical resonance frequencies along the line A-A indicated in Figure 6, dots are data points and solid lines indicate linear fits to the data.

vertical mode. Since the sensitivity of the first vertical mode is relatively constant along the scan points, no rotation about the length axis is observed. However, for the second vertical mode, the qPlus sensors with larger tip masses show a sloped sensitivity across the line A-A, indicating that the eigenmode includes some torsional rotation of the prong. The indication of torsional rotation for the glue-only qPlus sensor is believed to be due to asymmetric distribution of the glue.

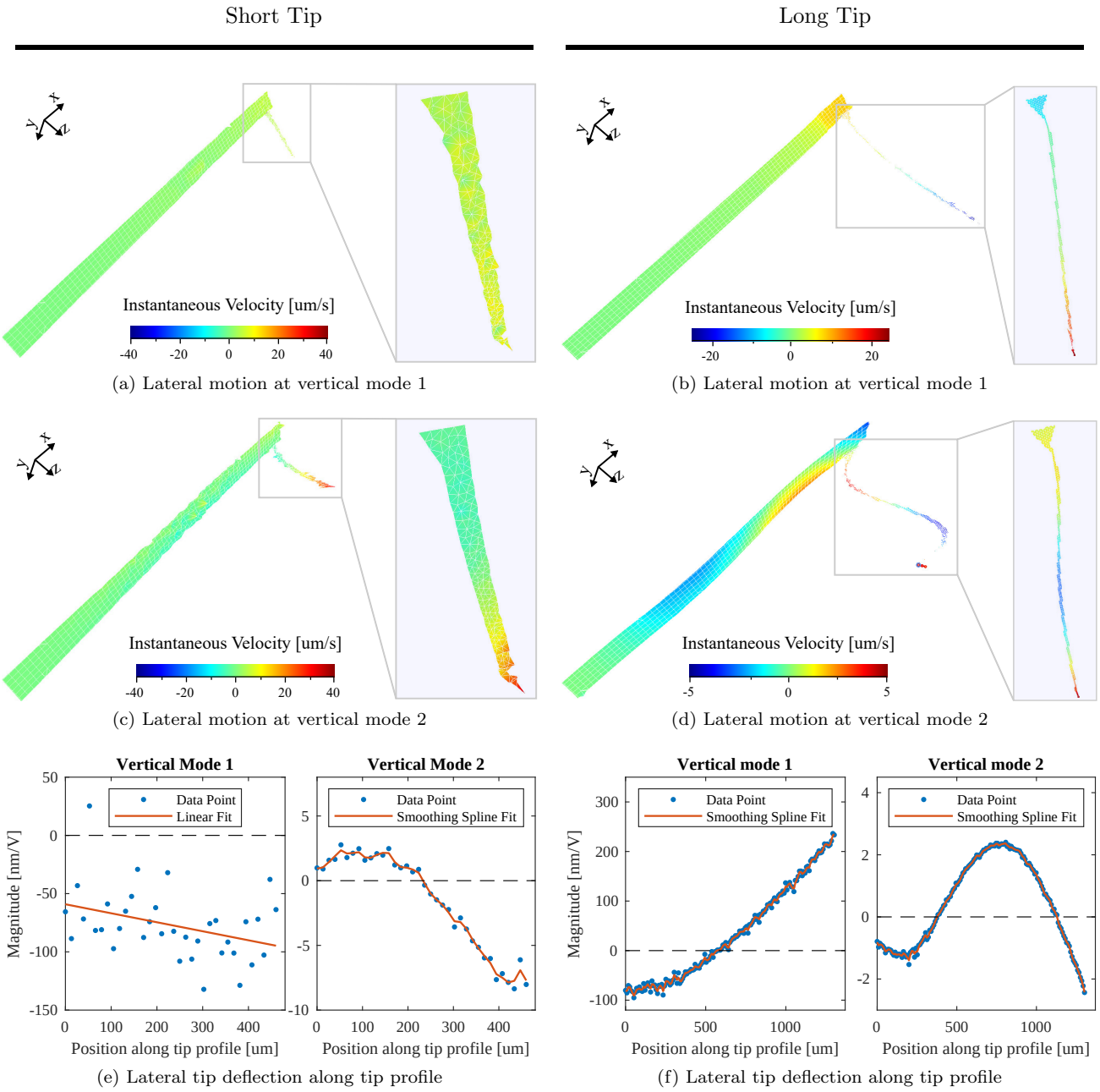

(a) Lateral motion at vertical mode 1

(b) Lateral motion at vertical mode 1

(c) Lateral motion at vertical mode 2

(d) Lateral motion at vertical mode 2

(e) Lateral tip deflection along tip profile

(f) Lateral tip deflection along tip profile

Figure 10. Experimental lateral deflection of the first and second vertical mode of the short-tip and long-tip qPlus sensors under electrical excitation. Lateral 3D mode shapes of the (a)-(b) first and (c)-(d) second vertical mode, the inset shows a zoom mode shape scan of the tip only. The legend corresponds to the inset. (e)-(f) Tip profile extracted along the tip scan points of the first and second vertical mode.

4.5. Lateral Tip Deflection

To investigate the torsional rotation of the prong at the first and second vertical mode and the resulting lateral tip deflection, high-resolution scans of the qPlus sensors from the side, and along the tip were performed. These lateral deflection at the first and second vertical mode of the short-tip and long-tip qPlus sensor are shown in Figure 10. By evaluating the frequency responses along the tip profile line indicated in Figure 6, the mode shapes of the tips are observed.

From Figure 10(a), it can be seen that the short-tip qPlus sensor prong and the tip do not show significant lateral motion at the first vertical mode. In contrast, the short tip shows significant lateral deflection at the second eigenmode as observed in Figure 10(c). The lateral deflection profile of the short tip is plotted in Figure 10(e). While the first vertical mode tip profile does not show significant deflection,

the second vertical mode tip profile has a significant deflection at the resonance frequency.

From Figure 10(b) and (d), it can be seen that the long-tip qPlus sensor prong and the tip show significant lateral motion at the first and second vertical mode. The lateral deflection profile of the long tip is plotted in Figure 10(f). In this case, the tip mode shapes show significant deflection at the first and second vertical modes.

4.6. Discussion

By comparing the vertical and lateral frequency responses of the first and second vertical modes, the ratio of lateral to vertical tip deflection can be determined. For the short-tip qPlus sensor at the first vertical mode, no significant tip deflection is observed and the lateral tip deflection is less than 10% of the vertical deflection. In contrast, the lateral deflection at the second vertical mode is around 80% of the vertical deflection.

For the long-tip qPlus sensor, the lateral deflection is around 30% of the vertical deflection at the first vertical mode, and 175% at the second vertical mode. This highlights the fact that lateral tip deflection becomes significant for larger tip geometries and at higher eigenmodes of the qPlus sensor.

The above conclusion is further confirmed by plotting the simulated and experimental tip deflection of the short-tip and long-tip qPlus sensors at the first vertical, second lateral, and second vertical mode, in Figure 11. The lateral tip deflection profiles are extracted along the finite element mesh nodes of the tip and normalized. The finite element analysis in Figure 11(a) predicts that the long-tip qPlus sensor shows increased lateral deflection of the tip for the first and second vertical mode as well as the second lateral bending mode. The predicted tip profiles are closely reproduced by the normalized experimental deflection profiles measured along the tip of the short-tip and long-tip qPlus sensors in Figure 11(b). Note that due to the normalization, the tip deflection at the vertical first mode of the short-tip qPlus sensor are exaggerated and would otherwise appear as flat lines in Figure 11.

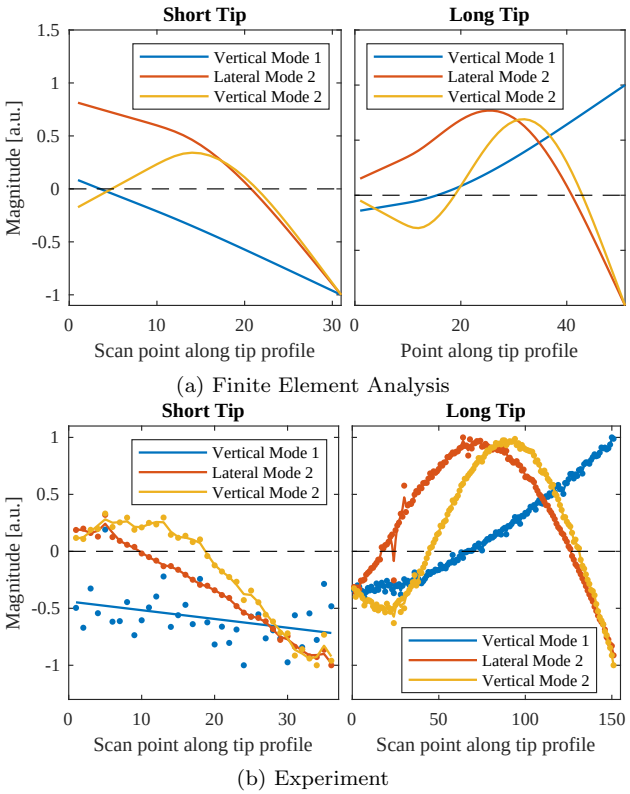

Figure 11. Normalized lateral tip deflection of the first vertical, first lateral and second vertical mode. Lateral tip deflection along the tip profile from (a) finite element analysis and (b) experiment. The predicted tip profiles from finite element analysis are closely reproduced by the normalized experimental deflection profiles.

5. Conclusion

This work presents a detailed analysis of the tip vibration characteristic of qPlus sensors that are commonly employed for high resolution AFM measurements. Next to the first vertical eigenmode, which is commonly excited and read-out during AFM operation, particular attention is put on the second lateral and the second vertical eigenmodes. Recently, it was demonstrated that the internal chemical structure of individual adsorbed molecules can be visualized using higher eigenmodes of qPlus sensors via the bond imaging technique. Hence, multifrequency imaging schemes [37–40] become possible that may lead to decreased data acquisition times and/or increased force sensitivity. Therefore, characterization of vibration at higher eigenmodes is important for interpreting the image contrast. We found that even for relatively short tips there can be a significant amount of lateral tip deflection (up to 80%) in the second vertical eigenmode. For larger tips, a lateral portion on the order of 175% was observed in the second vertical eigenmode. Lateral tip translation of this magnitude will strongly affect the AFM image contrast. In case of the second lateral mode, the tip translation is almost exclusively in the lateral direction, which is very promising for performing lateral force microscopy. Furthermore, the findings also have implications for the conventional AFM operation at the first vertical eigenmode. Depending on the length of the tip, lateral tip translation on the order of 10 - 30% are observed. To minimize this as much as possible, the tip length and mass should be kept as small a possible. The authors are currently working on a detailed analysis

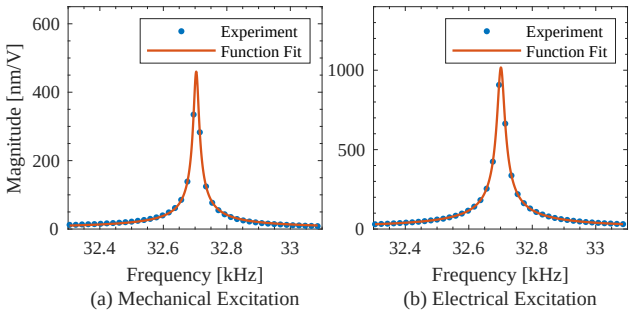

Figure A1. Magnitude Response and Lorentzian function fit for Q factor identification Magnitude response of the first vertical mode of the tip-less qPlus sensor under (a) mechanical excitation and (b) electrical excitation and function fit to Equation A.2.

of the bond imaging AFM contrast at different lateral and vertical eigenmodes.

Acknowledgements

M. G. Ruppert and D. Ebeling wish to acknowledge the funding support from the German Research Foundation (Deutsche Forschungsgemeinschaft, DFG) under the category 'Initiation of International Collaborations' with reference EB 535/2-1.

Appendix A. Q-factor Identification

When the qPlus sensors are actively driven at resonance, the transfer function from actuation voltage to tip deflection is given by

$$G(s) = \frac{\alpha\omega_0^2}{s^2 + \frac{\omega_0}{Q}s + \omega_0^2} \tag{A.1}$$

and has units of [m/V] where α is the DC-gain, ω_0 the resonance frequency and Q the quality factor. Then, the magnitude response of the transfer function is given by the Lorentzian-shaped function [41]

$$|G(j2\pi f)| = \sqrt{\frac{\alpha^2}{(1-\frac{f^2}{f_0^2})^2 + \frac{f^2}{f_0^2 Q^2}}} \tag{A.2}$$

which can be used to fit to the experimentally obtained magnitude response. From the fit, the resonance frequency, Q factor and sensitivity can be obtained even if the recorded responses is under-sampled at the resonance as is shown in Figure A1.

The identified Q factors of the first and second vertical resonance frequencies of the qPlus sensors from mechanical and electrical excitation are stated in Table A1. Note that the different transduction methods yield different Q factors but the general trend is preserved.

Table A1. Quality factors of the first and second vertical resonance frequencies of the qPlus sensors from mechanical and electrical excitation.

	Mechanical		Electrical	
Sensor	$Q_{1,v}$	$Q_{2,v}$	$Q_{1,v}$	$Q_{2,v}$
Tip-less	1867	821.5	1399	1125
Glue	2097	615.0	1442	872.2
Short Tip	1646	585.0	1263	374.9
Long Tip	512.7	298.3	532.8	367.0

Appendix B. Modal Stiffness Identification

Appendix B.1. Experimental

The modal stiffnesses of the qPlus sensors are experimentally determined using the thermal noise method [42]. For this purpose, the piezoelectric stack actuator and all qPlus sensor electrodes are grounded and the velocity power spectrum at the end of the free prong is measured using the laser Doppler vibrometer. The thermal stiffness at each mode is obtained by performing a Lorentzian function fit to the measured thermal noise response of the form [30, 43]

$$S(f) = \frac{Af_0^4}{Q^2(f^2 - f_0^2)^2 + f^2 f_0^2} + A_0, \tag{B.1}$$

where A is a fitting parameter and A_0 is the white background noise. From the fit, the mean squared velocity can be extracted as

$$\bar{v}^2 = \frac{\pi f_0 A}{2Q} \tag{B.2}$$

which allows to calculate the spring constant as

$$k = (2\pi f_0)^2 \frac{k_B T}{\bar{v}^2}. \tag{B.3}$$

The resulting spectra and the corresponding Lorentzian function fits are shown in Figure B1. The modal stiffnesses of the first and second vertical mode are summarized in Table B1. It appears that the first mode stiffness remains constant irrespective of the added tip mass which is consistent with [25]. In contrast, the second eigenmode stiffness is extremely large and can only be measured for the tip-less and glue-only qPlus sensor. It appears that the stiffness increases rapidly which makes the thermal noise response at the second mode unmeasurable for the qPlus sensors with short and long tip which is also consistent with [25].

Appendix B.2. Finite Element Analysis

The modal stiffness is calculated using modal analysis and $k_i = \omega_i^2 m_i$, where ω_i is the resonance frequency and m_i is the modal mass of the i^{th} mode [44]. Values for the resonance frequencies and modal masses are directly extracted from the solved model in ANSYS

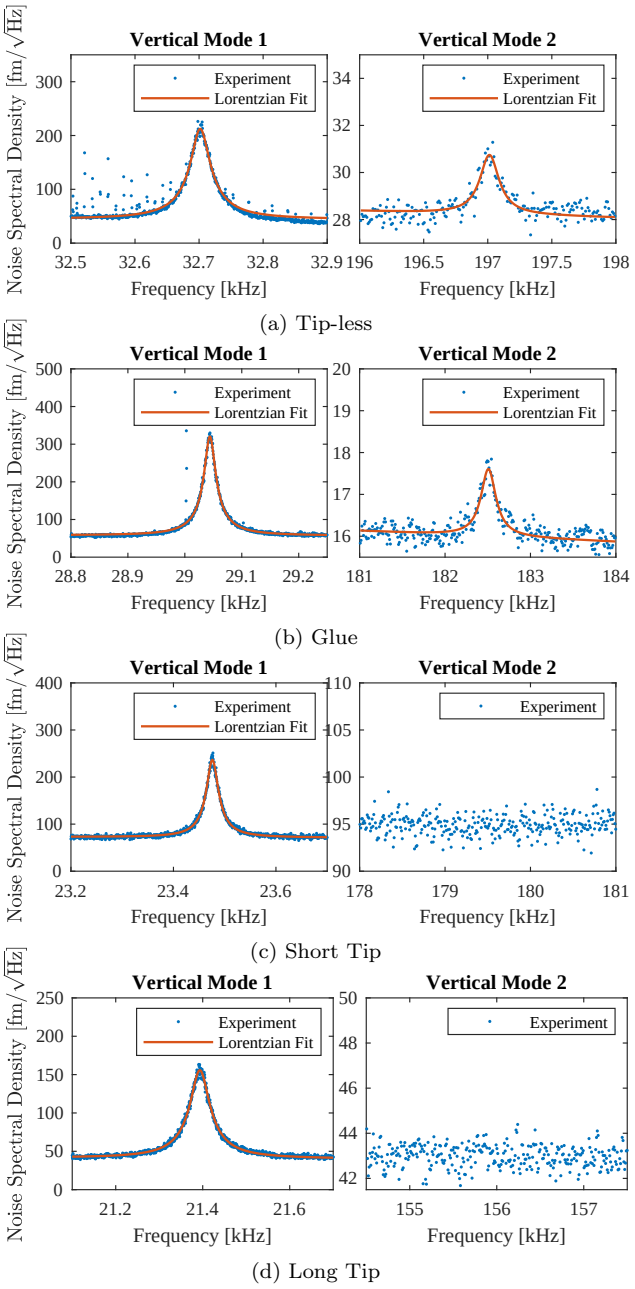

Figure B1. Thermal noise measurement of the qPlus sensors. The experimental thermal noise spectra and corresponding Lorentzian function fits to Equation B.1 to the first and second vertical modes allow the extraction of the dynamic stiffnesses. For the sensors with attached tip (c) and (d), the second eigenmode is too stiff to be measured.

[45]. The resulting modal stiffnesses are listed in Table B1.

Table B1. Simulated and experimentally determined first and second vertical mode dynamic stiffnesses of the qPlus sensors.

Sensor	Simulation		Experiment	
	$k_{1,v}$ [kHz]	$k_{2,v}$ [kHz]	$k_{1,v}$ [kHz]	$k_{2,v}$ [kHz]
Tip-less	2261	85,431	2,060	98,299
Glue	2248	85,531	1,358	232,086
Short Tip	2205	114,760	2,235	N/A
Long Tip	2281	139,170	2,643	N/A

[1] Binnig G, Quate C F and Gerber C 1986 *Phys. Rev. Lett.* **56**(9) 930–933 URL http://link.aps.org/doi/10.1103/PhysRevLett.56.930

[2] Gross L, Mohn F, Moll N, Liljeroth P and Meyer G 2009 *Science* **325** 1110–1114

[3] Ebeling D, Šekutor M, Stiefermann M, Tschakert J, Dahl J E, Carlson R M, Schirmeisen A and Schreiner P R 2018 *Nature Communications* **9**

[4] Parsons E S, Stanley G J, Pyne A L, Hodel A W, Nievergelt A P, Menny A, Yon A R, Rowley A, Richter R P, Fantner G E *et al.* 2019 *Nature Communications* **10** 2066

[5] Zhang J, Chen P, Yuan B, Ji W, Cheng Z and Qiu X 2013 *Science* **342** 611–614 (*Preprint* https://www.science.org/doi/pdf/10.1126/science.1242603) URL https://www.science.org/doi/abs/10.1126/science.1242603

[6] de Oteyza D G, Gorman P, Chen Y C, Wickenburg S, Riss A, Mowbray D J, Etkin G, Pedramrazi Z, Tsai H Z, Rubio A, Crommie M F and Fischer F R 2013 *Science* **340** 1434–1437 (*Preprint* https://www.science.org/doi/pdf/10.1126/science.1238187) URL https://www.science.org/doi/abs/10.1126/science.1238187

[7] Gross L, Mohn F, Moll N, Schuler B, Criado A, Guitián E, Peña D, Gourdon A and Meyer G 2012 *Science* **337** 1326–1329 (*Preprint* https://www.science.org/doi/pdf/10.1126/science.1225621) URL https://www.science.org/doi/abs/10.1126/science.1225621

[8] Mönig H, Amirjalayer S, Timmer A, Hu Z, Liu L, Arado O D, Cnudde M, Strassert C A, Ji W, Rohlfing M *et al.* 2018 *Nature Nanotechnology* **13** 371–375

[9] Ellner M, Pou P and Perez R 2019 *ACS nano* **13** 786–795

[10] Riss A, Paz A P, Wickenburg S, Tsai H Z, De Oteyza D G, Bradley A J, Ugeda M M, Gorman P, Jung H S, Crommie M F *et al.* 2016 *Nature Chemistry* **8** 678–683

[11] Zint S, Ebeling D, Schlöder T, Ahles S, Mollenhauer D, Wegner H A and Schirmeisen A 2017 *ACS nano* **11** 4183–4190

[12] Ebeling D, Zhong Q, Schlöder T, Tschakert J, Henkel P, Ahles S, Chi L, Mollenhauer D, Wegner H A and Schirmeisen A 2018 *ACS nano* **13** 324–336

[13] Huber F, Berwanger J, Polesya S, Mankovsky S, Ebert H and Giessibl F J 2019 *Science* **366** 235–238

[14] Zhong Q, Ihle A, Ahles S, Wegner H A, Schirmeisen A and Ebeling D 2021 *Nature Chemistry* **13** 1133–1139

[15] Albrecht T, Grütter P, Horne D and Rugar D 1991 *J. Appl. Phys.* **69** 668–673

[16] Giessibl F J 1998 *Appl. Phys. Lett.* **73** 3956–3958 (*Preprint* https://doi.org/10.1063/1.122948) URL https://doi.org/10.1063/1.122948

[17] Giessibl F J, Bielefeldt H, Hembacher S and Mannhart J 1999 *Applied Surface Science* **140** 352–357 ISSN 0169-4332 URL https://www.sciencedirect.com/science/article/pii/S0169433298005534

[18] Giessibl F J, Hembacher S, Herz M, Schiller C and Mannhart J 2004 *Nanotechnology* **15** S79–S86 URL https://doi.org/10.1088/0957-4484/15/2/017

[19] Martin-Jimenez D, Ahles S, Mollenhauer D, Wegner H A,

Schirmeisen A and Ebeling D 2019 *Phys. Rev. Lett.* **122**(19) 196101 URL https://link.aps.org/doi/10.1103/PhysRevLett.122.196101

[20] Kawai S, Glatzel T, Koch S, Such B, Baratoff A and Meyer E 2009 *Phys. Rev. Lett.* **103**(22) 220801 URL https://link.aps.org/doi/10.1103/PhysRevLett.103.220801

[21] Ebeling D and Solares S D 2013 *Nanotechnology* **24** 135702 URL https://doi.org/10.1088/0957-4484/24/13/135702

[22] Bettac A, Koeble J, Winkler K, Uder B, Maier M and Feltz A 2009 *Nanotechnology* **20** 264009 URL https://doi.org/10.1088/0957-4484/20/26/264009

[23] Ooe H, Kirpal D, Wastl D S, Weymouth A J, Arai T and Giessibl F J 2016 *Appl. Phys. Lett.* **109** 141603 (*Preprint* https://doi.org/10.1063/1.4964125) URL https://doi.org/10.1063/1.4964125

[24] Yamada Y, Ichii T, Utsunomiya T and Sugimura H 2019 *Jpn. J. Appl. Phys.* **58** 095003

[25] Tung R C, Wutscher T, Martinez-Martin D, Reifenberger R G, Giessibl F and Raman A 2010 *J. Appl. Phys.* **107** 104508 (*Preprint* https://doi.org/10.1063/1.3407511) URL https://doi.org/10.1063/1.3407511

[26] Ebeling D, Zhong Q, Ahles S, Chi L, Wegner H A and Schirmeisen A 2017 *Appl. Phys. Lett.* **110** 183102 (*Preprint* https://doi.org/10.1063/1.4982801) URL https://doi.org/10.1063/1.4982801

[27] Weymouth A J, Riegel E, Gretz O and Giessibl F J 2020 *Phys. Rev. Lett.* **124**(19) 196101 URL https://link.aps.org/doi/10.1103/PhysRevLett.124.196101

[28] Kirpal D, Qiu J, Pürckhauer K, Weymouth A J, Metz M and Giessibl F J 2021 *Rev. Sci. Instrum.* **92** 043703 (*Preprint* https://doi.org/10.1063/5.0041369) URL https://doi.org/10.1063/5.0041369

[29] Rothberg S, Allen M, Castellini P, Maio D D, Dirckx J, Ewins D, Halkon B, Muyshondt P, Paone N, Ryan T, Steger H, Tomasini E, Vanlanduit S and Vignola J 2017 *Optics and Lasers in Engineering* **99** 11 – 22 ISSN 0143-8166 URL http://www.sciencedirect.com/science/article/pii/S0143816616303724

[30] Ruppert M G, Bem N F S D, Fleming A J and Yong Y K 2021 *Characterization of Active Microcantilevers Using Laser Doppler Vibrometry* vol 2 (Sydney, Australia: Springer International Publishing) chap 45

[31] Giessibl F J 2019 *Rev. Sci. Instrum.* **90** 011101 (*Preprint* https://doi.org/10.1063/1.5052264) URL https://doi.org/10.1063/1.5052264

[32] Huber F and Giessibl F J 2017 *Rev. Sci. Instrum.* **88** 073702 (*Preprint* https://doi.org/10.1063/1.4993737) URL https://doi.org/10.1063/1.4993737

[33] Preumont A 2006 *Mechatronics: Dynamics of Electromechanical and Piezoelectric Systems* vol 136 (Springer Netherlands) ISBN 978-1-4020-4695-7

[34] Moore S I, Ruppert M G and Yong Y K 2017 *Beilstein Journal of Nanotechnology* **8** 358–371 ISSN 2190-4286

[35] Ruppert M G, Moore S I, Zawierta M, Fleming A J, Putrino G and Yong Y K 2019 *Nanotechnology* **30** 085503 URL http://iopscience.iop.org/article/10.1088/1361-6528/aae40b

[36] Kim B, Jahng J, Khan R M, Park S and Potma E O 2017 *Phys. Rev. B* **95**(7) 075440 URL https://link.aps.org/doi/10.1103/PhysRevB.95.075440

[37] Guo S, Solares S D, Mochalin V, Neitzel I, Gogotsi Y, Kalinin S V and Jesse S 2012 *Small* **8** 1264–1269

[38] Garcia R 2020 *Chemical Society Reviews* **49** 5850–5884

[39] Eichhorn A L and Dietz C 2021 *Advanced Materials Interfaces* **8** 2101288

[40] Rajabifar B, Bajaj A, Reifenberger R, Proksch R and Raman A 2021 *Nanoscale* **13** 17428–17441

[41] Ruppert M G, Bartlett N J, Yong Y K and Fleming A J 2020 *Sens. Actuators Phys.* **312** 112092 URL http://www.precisionmechatronicslab.com/wp-content/uploads/2020/09/J20f.pdf

[42] Butt H J and Jaschke M 1995 *Nanotechnology* **6** 1 URL http://stacks.iop.org/0957-4484/6/i=1/a=001

[43] Sader J E, Sanelli J A, Adamson B D, Monty J P, Wei X, Crawford S A, Friend J R, Marusic I, Mulvaney P and Bieske E J 2012 *Rev. Sci. Instrum.* **83** 103705 URL http://scitation.aip.org/content/aip/journal/rsi/83/10/10.1063/1.4757398

[44] Fu Z F and He J 2001 *Modal Analysis* 1st ed (Elsevier Science & Technology) ISBN 9780750650793

[45] Ansys Inc 2021 *ANSYS Mechanical APDL Theory Reference, Release 2021 R2, Chapter 15*